-RESEARCH PAPER-

International Journal of Mining and Geo-Engineering

IJMGE

IJMGE 57-3 (2023) 241-250

DOI: 10.22059/IJMGE.2023.354047.595024

A potential field geophysical study to image a Potash resource through Depth from Extreme Points (DEXP) automatic transformation technique, a case study of Ghareh-Aghaj deposit in NW of Iran

Mahya Mehrvash [a], Maysam Abedi [a,*], Gholam-Hossain Norouzi [a]

[a] *School of Mining Engineering, University of Tehran, Tehran, Iran.*

Article History:

Received: 19 January 2023.

Revised: 24 February 2023.

Accepted: 04 March 2023.

ABSTRACT

Utilizing magnetic susceptibility and density contrast models, the primary aim of analyzing potential field data is to determine essential source parameters, including depth, structural index, horizontal expansion, and physical characteristics. In geophysical explorations, the accurate determination of subsurface depth is of utmost importance. This study employs the Depth from Extreme Points (DEXP) automatic transformation technique to interpret potential field data. DEXP relies on the precise analysis of local wavenumbers at different scales and the extreme points of the DEXP field to extract source depth, horizontal position, and structural index. This method is highly stable and less sensitive to noisy data due to the inclusion of an upward continuation filter and a potential field derivative operator. Additionally, the results are more reliable compared to alternative techniques. Moreover, the DEXP method is fully automated and does not require prior knowledge of the data collection area, making it a rapid imaging approach. As multiscale methods are less reliant on magnetic induction fields, they have become increasingly popular in magnetic field computations. To validate the proposed approach, synthetic scenarios are initially simulated. Subsequently, the DEXP technique is applied to demonstrate the depth extension of assumed models using synthetic gravity and magnetic data. This method is then implemented on data from the Ghareh-Aghaj potash exploratory area in Zanjan Province, Iran. The outcomes indicate that the potash deposit has minimal lateral expansion and is more pronouncedly extended in depth. Notably, these findings exhibit a satisfactory level of agreement with results obtained from exploratory borehole investigations.

Keywords: *Automatic DEXP transformation, Multiscale methods, Potential field, Depths estimate.*

1. Introduction

To comprehend the characteristics of field-originating sources, including their position, geometrical structure, and physical properties contrast (magnetic susceptibility and density), it becomes imperative to analyze potential field data, encompassing both magnetic and gravity aspects. The analysis of data gathered from airborne, marine, and terrestrial surveys, when carried out through inversion techniques, often consumes significant time due to the substantial data volume. Consequently, over the years, several automated and semi-automated methods have been devised to swiftly and accurately assess source properties [1]. Numerous techniques for approximating depth have been established, including the analytical signal method [2], source parameter image technique [3], upward continuation of scattered potential field data [4], Euler deconvolution [5-7], deconvolution analytical signal [8], and enhanced local wavenumber technique [9]. These approaches, which do not rely heavily on magnetic susceptibility, frequently prove effective for sources with simple geometrical shapes. As such, initiating an initial understanding of potential field structure through depth assessment provides valuable preliminary insights into the core attributes of the intended source.

Moreover, magnetic depth estimation holds particular significance in the delineation of faults, contact interfaces, folds, and salt formations, primarily due to the expeditious nature and relatively lower expenses associated with semi-automated methodologies. During the 1970s, automated methods for depth estimation supplanted graphical techniques. These methodologies often leverage field-oriented derivatives. Thompson (1982) and Reid et al. (1990) [5-6] introduced Euler's technique grounded in employing first-field derivatives for both two-dimensional and three-dimensional contexts. A notable advantage of employing such methods is their inherent ability to autonomously identify the source's location. Nevertheless, this necessitates the provision of the geometrical structure's form as foundational data.

The Source Parameter Imaging (SPI) technique was formulated by Thurston and Smith in 1997 [3]. Leveraging the concept of local wavenumber, the depth of the field structure is ascertained through the consideration of the second derivative [8]. The iterative SPI (iSPI) method, an evolved rendition of the prior technique, was introduced by Smith et al. in 1998, boasting the additional capability of structural index quantification [10]. An enhanced iteration of the local wavenumber approach (ELW), devised by Salem et al. (2005), employs the concept of local wavenumber in conjunction with Euler's equations to determine source location and type [9].

It's worth noting that each of these techniques exhibits considerable sensitivity to data noise, necessitating data of sufficiently high quality for the generation of precise outcomes. Recent years have witnessed the emergence of multiscale methodologies for source feature estimation [11-14].

This research examines the multiscale analysis method of DEXP automatic transformation on potential field data for potash in Ghareh-

* Corresponding author: *E-mail address:* maysamabedi@ut.ac.ir (M. Abedi).

Aghaj, an area situated in the northern region of the Zanjan Province. To achieve this goal, we will first investigate synthetic structures considered to be relatively complex. Next, applying this procedure to the real data analyses its result to determine the most accurate interpretation.

2. Depth from extreme points

In recent years, the advent of multiscale methodologies has been spurred by the observation that potential fields generated by ideal sources like dikes and cylinders exhibit homogeneity, and their variations are linked to a specific power of the distance from the source. Capitalizing on this characteristic, probing the field at various scales imparts valuable insights into source depth and structure [11]. Among these multiscale approaches, the focus of this article centers on the multiscale analysis of potential fields employing the automated DEXP transformation for depth estimation, utilizing the local wave number [14]. This automated technique offers a rapid and facile means of appraising source parameters from magnetic and gravity survey data.

The DEXP transformation method is rooted in the scaling of the potential field, denoted as 'f', at differing heights (scales) using an appropriate exponent associated with that scale. This scaling operation, termed the Scaling Function (Scale Fun), is contingent on the height, scaling exponent (henceforth referred to as structural index), and field order. Thus, the DEXP transformation of the potential field is computed as per Equation (1) [11]:

$$DEXP(h_i) = |h_i|^{\alpha} f(x,y,z)_{z=h_i} = |h_i|^{\frac{N}{2}} f(x,y,z)|_{z=h_i} i = 1,2,\dots,l \quad (1)$$

h_i represents the scale, or the height used to conduct the upward continuation filter, and l is the number of scales to produce the DEXP field. Several techniques exist for estimating the structural index, or alternatively, a fitting value can be ascribed based on other pertinent area-specific data. Demonstrating the effectiveness of this approach, when the scaling exponent is judiciously chosen, the minimum or maximum values within the DEXP field align with the positions of potential field sources. In situations where the interference effects stemming from proximate sources or the pervasive regional field are substantial, field derivatives can be effectively employed. In such instances, the DEXP transformation of the nth-order derivative of the field is computed using the overarching Equation (2) [13]:

$$DEXP(h_i) = |h_i|^{\alpha_n} \frac{\partial^n f(x,y,z)}{\partial z^n} | z = h_i = |h_i|^{\frac{(N+n)}{2}} \frac{\partial^n f(h_i)}{\partial z^n} | z = h_i i = 1,2,\dots,l \quad (2)$$

Elevating the order of the field derivative enhances the resolution for surface-level sources while providing lower resolution for deeper sources. When the scaling exponent, and consequently, the structural index, are accurately integrated into the DEXP transformation, slight adjustments in the order of derivation lead to subtle shifts in the positions of extreme points and consequently, in the depth determination of sources. It is noteworthy to emphasize that this degree of invariance is more pronouncedly accurate and precise when applied to sources characterized by simplistic shapes or those closely aligned with ideal source characteristics.

Given the inherent stability and reliability of the upward continuation process, the DEXP transformation likewise exhibits resilience against data noise, even in scenarios involving high-order derivatives. Specifically, due to the bipolar attributes of magnetic sources, the DEXP transformation demonstrates alternating positive and negative values when the source is positioned within this interval. Consequently, deducing the attributes of the desired source becomes challenging. In such instances, for enhanced precision in source localization, it proves advantageous to leverage the DEXP profile amplitude or field amplitude modulation, commonly referred to as the Root Sum of Squares [11].

In such scenarios, the bipolar characteristic of the DEXP field is mitigated, revealing a solitary maximum point. Notably, the latter two metrics display minimal reliance on the magnetization direction, thereby augmenting the precision of source position estimation. As previously highlighted, the paramount advantage of multiscale methodologies lies in their rapid computational capabilities. Unlike inversion techniques, these approaches facilitate the efficient analysis of extensive data volumes or even expedite the visualization of sources [11].

The automated DEXP transformation, anchored in the local wavenumber function, serves as the foundational underpinning. This transformation is adept at deducing the source's depth, position, and structural index, affording the ability to appraise source characteristics without necessitating preliminary information.

In the following equation, the first-order local wavenumber k_1 of a potential field f, for two-dimensional sources is defined as the rate of change of the local phase of the analytic signal [15]:

$$k_1 = \frac{\partial}{\partial x} tan^{-1}\left(\frac{\frac{\partial f}{\partial z}}{\frac{\partial f}{\partial x}}\right) \quad (3)$$

The local wavenumber of the magnetic field for two-dimensional sources at a horizontal position x_0 and a depth z_0 can be written as [10]:

$$k_1(x,z) = -\frac{(N+1)(z-z_0)}{(x-x_0)^2+(z-z_0)^2} \quad (4)$$

Where N is the structural index, a quantity related to the source geometry [5], assuming, in the magnetic case, the integer values 0, 1, and 2 for contact, dike, and horizontal cylinder models, respectively. The second-order local wavenumber can be written as [10]:

$$k_2 = \frac{\partial}{\partial x} tan^{-1}\left(\frac{\frac{\partial^2 f}{\partial z^2}}{\frac{\partial^2 f}{\partial x \partial z}}\right) = -\frac{(N+2)(z-z_0)}{(x-x_0)^2+(z-z_0)^2} \quad (5)$$

In addition, this relationship can be extended to higher-order versions of local wavenumbers by generalizing Eqs. (4) and (5) [14]:

$$k_p(x,z) = \frac{\partial}{\partial x} tan^{-1}\left(\frac{\partial^p f}{\partial z^p} / \frac{\partial^p f}{\partial x \partial z^{p-1}}\right) = -\frac{N_p(z-z_0)}{(x-x_0)^2+(z-z_0)^2} \quad (6)$$

Where p is the order of the local wavenumber and Np=N+p. [14]. Additionally, according to the definition of the scaling function τ_n in Equation (7), conducts as the logarithmic derivative of a potential field f_p with respect to log (z) [11]:

$$\tau = \frac{\partial\, log(f_p)}{\partial\, log(z)} = -N_p \frac{z}{z-z_0} \quad (7)$$

Likewise, by computing the scaling function for the local wavenumber k_p [14]:

$$\tau(k_p) = \frac{\partial\, log(k_p)}{\partial\, log(z)} = -\frac{z}{z-z_0} \quad (8)$$

This correlation underscores that the scaling function derived from the local wavenumber, in contrast to the scaling function derived from the potential field, remains unaffected by the source's structural index. Upon performing the requisite mathematical derivations [11,14], the DEXP transformation of the local wavenumber pertaining to the p-order is acquired by using Equation (9):

$$\Omega_p = z^{0.5} k_p \quad (9)$$

In a similar way to the approach by Fedi (2007) [11], where it's mentioned that at z = - z0, τ = - 0.5, similar to the DEXP transformation applied to the potential fields, the highest or lowest values of Ω_p will match the positions of potential sources. By merging Equations (8) and (9) at the highest point of DEXP, known as Ω_{max} and located at (x, z) = (x0, -z0), it's also easy to estimate the source's structural index as established in Equation (10):

$$N = 2z_0^{0.5} \Omega_{max} \quad (10)$$

This method can be developed for a three-dimensional case by implementing the proper formulation of the local wavenumber [16]. In the next phases, the capabilities and advantages of this method will be proven practically by applying the automatic DEXP transformation technique on synthetic potential field data such arised from sources like dike and cylinder.

3. Forward modeling of simple-shaped sources

The magnetic anomaly produced by a thin dike exhibiting substantial longitudinal and depth extension, perpendicular to the measurement axis, can be acquired through Equation (11) [2, 17-18]:

$$\Delta T(x,z) = \frac{A(x-x_0)+B(z-z_0)}{(x-x_0)^2+(z-z_0)^2} \quad (11)$$

Here, x denotes the measurement point, x_0 represents the horizontal position of the dike in relation to the origin, and z_0 signifies the distance to the dike's surface. Indeed, Equations (12) and (13) are employed to ascertain the values of A and B, both contingent upon the physical characteristics of the dike:

$$A = -2c_m J \Delta x(\alpha \cos\phi + \beta \sin\phi) \quad (12)$$

$$B = -2c_m J \Delta x(\alpha \sin\phi + \beta \cos\phi) \quad (13)$$

Here, J signifies the magnetization, Δx stands for the thickness of the dike, Φ denotes the slope angle of the dike, and cm represents the magnetic constant. In the emu unit system, the value and unit of cm are both one, which, in the SI system, equates to:

$$c_m = \frac{\mu_0}{4\pi} = 10^{-7} \quad (14)$$

α and β describe directional quantities depending on the field and orientation related to the magnetization process:

$$\alpha = F_x J_x - F_z J_z \quad (15)$$

$$\beta = F_x J_z + F_z J_x \quad (16)$$

Given that the assessment axis aligns with the north direction (where the azimuth of the x-axis equals zero), Equations (17) and (18) are pertinent to vectors oriented along the principal field and magnetization directions:

$$\hat{F} = F_x\hat{\imath} + F_z\hat{k} = \cos I \cos D\,\hat{\imath} + \sin I\,\hat{k} \quad (17)$$

$$\hat{J} = J_x\hat{\imath} + J_z\hat{k} = \cos I' \cos D'\hat{\imath} + \sin I'\hat{k} \quad (18)$$

Here, I and D represent the inclination and declination angles of the field, while I' and D' indicate the inclination and declination angles of magnetization. Assuming an inductive magnetization of the dike, with $D = D'$ and $I = I'$, the magnetization vector and earth field vector align harmoniously.

Hence, for each thin dike, the magnetic anomaly of the overall field intensity can be established, considering its specific parameters. Furthermore, the gravity anomaly gz corresponding to thin dikes is derived through Equation (19) (Telford, 1990):

$$g = 4.07\times10^{-3}\sigma\left[\frac{x}{2}log\left(\frac{D^2+x^2}{d^2+x^2}\right) + D\left\{\frac{\pi}{2} + tan^{-1}\left(\frac{x}{D}\right)\right\} - d\left\{\frac{\pi}{2} + tan^{-1}\left(\frac{x}{d}\right)\right\}\right] \quad (19)$$

Where, D signifies the vertical distance from the horizon to the lower depth of the dike, and d represents the vertical distance from the horizon to the upper depth of the dike.

Moreover, the magnetic anomaly stemming from an infinitely longitudinally extended horizontal cylinder, uniformly magnetized, corresponds to the linear magnetic field of dipoles, as derived from Equation (20) [19]:

$$\vec{B} = \frac{2c}{r^4}(2(\vec{m}.\vec{r})\vec{r} - r^2\vec{m}) \quad (20)$$

Here, m signifies the magnetic dipole moment per unit length (ampere per meter), and as per Equation (21), a designates the radius of the cylindrical section.

$$\vec{m} = \pi a^2\vec{J} \quad (21)$$

So r indicates the distance between the cylinder's axis and the measurement point, and J represents the magnetization intensity. Equation (22) can be deduced by considering that the distance to the axis of the cylinder is denoted as z_0, and its horizontal distance from the point of assessment origin is represented by x_0.

$$\vec{r} = (x-x_0)\vec{\imath} + (z-z_0)\vec{k} \quad (22)$$

According to its components, Equation (20) can be extended as seen in Equation (23):

$$\vec{B} = B_x\hat{\imath} + B_z\hat{k} = \frac{2c_m}{r^4}((2(m_x r_x + m_z r_z)r_x - m_x r^2)\hat{\imath} + (2(m_x r_x + m_z r_z)r_z - m_z r^2)\hat{k}) \quad (23)$$

At Equation (24), the vector m is determined, presuming the measurement axis directed to the north direction:

$$\vec{m} = m_x\hat{\imath} + m_z\hat{k} = m\cos I'\cos D'\hat{\imath} + m\sin I'\hat{k} \quad (24)$$

Equation (17) outlines the direction vector of the primary field, F, with I = I' and D = D' only when inductive magnetization prevails. Ultimately, Equation (25) is employed to calculate the magnetic anomaly of the cylinder at the position (x, z):

$$\Delta T(x,z) = \vec{B}.\hat{F} = B_x F_x + B_z F_z \quad (25)$$

By employing Equation (25), it becomes possible to ascertain the magnetic anomaly produced by each infinitely long horizontal cylinder at any point along the profile, given that all of its characteristics are known [10,19].

Moreover, the gravity anomaly, represented by the symbol gz for a horizontal cylinder, is akin to Equation (26) [19]:

$$g_z = -2\gamma\int_S \frac{\rho(S)}{r}\hat{r}\,dS \quad (26)$$

The vector $\hat{r}$denotes the cylinder's axis to the measurement point, and the value of gravity in the dS element, which is inversely correlated to distance, denoted by the $\rho(S)$.

4. Synthetic data simulation

Subsequently, basic geometric sources such as thin dikes and horizontal cylinders are employed to generate synthetic data through modeling, utilizing the provided method for magnetic and gravity models. Recognizing the inevitable presence of noise in real data, random Gaussian noise is introduced to the synthetic data to enhance the simulation. Following this, the DEXP transformation method is applied to these noisy datasets. The resulting responses are then compared with their actual values, representing the model parameters. Much like other techniques relying on field derivatives, the resolution and accuracy achieved with the DEXP method depends on the quality of the acquired data and the noise extent. The derivation process itself functions as a high-pass filter, significantly amplifying noise and surface anomalies. The introduction of noise not only distorts the results but also introduces instability. To mitigate the adverse influence of noise, we incorporate a low-pass filter. After a certain elevation, the responses stabilize through the upward continuation technique, with their variations becoming marginal. As a result, the target elevation becomes the threshold at which anomalies are mitigated, approaching the baseline value. For the validation of the DEXP approach using synthetic data, we employ two thin dikes that adapt to the criteria outlined in Table (1).

Figure 1(a) depicts the Bouguer observation of synthetic gravity data for two thin dikes, each accompanied by 2% random Gaussian noise. These dikes are positioned at (x_0, z_0) = (200,7) m and (x_0, z_0) = (400,10) m, and possess density contrasts of 1.2 and 1.5 g/cm^3, respectively. As illustrated in Figure 1(b), the accurate positioning of the DEXP transformation is evident for the two thin dikes, leading to the correct estimation of the source anomalies' depths. Next, it is essential to introduce a tapering effect on the data prior to applying the FFT technique to mitigate the Gibbs phenomenon, which arises from the Fourier transform used to approximate the field derivatives. The results for the two thin magnetic dikes with the specified parameters, as presented in Table (2), are illustrated in Figure 2.

Subsequently, the method was validated by analyzing the magnetic field of two vertical dikes. These dikes had magnetizations of 2 and 3A/m and were situated at positions (x0, z0) = (200, 20) m and (x0, z0) = (270,

30) m, respectively. The magnetic inclination and declination were set at 45° and 10°, respectively, while the measurement axis was oriented vertically to the structure. Despite the potential influence of interference effects on depth estimation, the outcome, as shown in Figure 2, reasonably corresponds to the known parameters of the model.

To mitigate the interference effect and enhance the resolution of the DEXP image, employing a higher-order local wavenumber proves advantageous. As previously mentioned, the DEXP transformation remains highly stable in relation to the differentiation order. The subsequent analysis in this study focuses on a synthetic model involving a horizontal cylinder, encompassing both magnetic and gravity data. Table (3) outlines the incorporation of noise into the synthetic gravity data of the horizontal cylinder to simulate real-world data scenarios.

Table 1. Characteristics for two thin dikes used to generate gravity data (all distances and angles are in meters and degrees, respectively).

Dike parameters	*Thin gravity dike No.1*	*Thin gravity dike No.2*
Distance between the depth and the surface of the dike (meters), z_0	7	10
Horizontal location relative to the origin (meters), x_0	200	400
Density contrast (g/cm^3)	1.2	1.5
Dike length	100	100
Transverse extension	50	50
Dike slope angle	90	90
Dike thickness (meters)	2	2
Structural index	1	1
Noise	Random, 2%	Random, 2%

Table 2. Characteristics for two thin dikes used to generate magnetic data (all distances and angles are in meters and degrees, respectively).

Dike parameters	*Thin dike No.1*	*Thin dike No.1*
Distance between the depth and the surface of the dike (meters), z_0	20	30
Horizontal position relative to the origin (meters), x_0	200	270
Magnetization (amps/meter)	2	3
The inclination angle of the earth field, I	45	45
Earth field declination angle, D	10	10
Total magnetization inclination, I'	45	45
Total magnetization declination angle, D'	10	10
Dike slope angle	90	90
Dike thickness (meters)	5	5
Noise	Random, 1%	Random, 1%

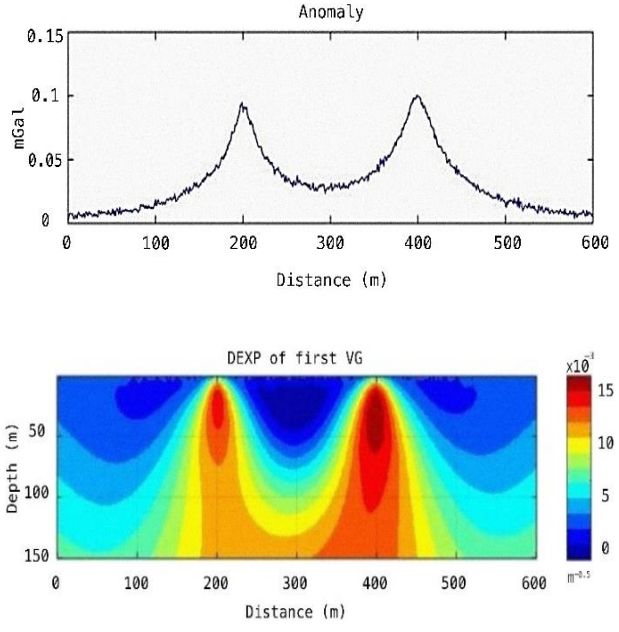

Figure 1. Synthetic gravity data of two thin dikes, (a) Bouguer observation, and (b) DEXP transformation. Observations were corrupted with 2% random Gaussian noise.

Table 3. Characteristics for a cylinder used to generate gravity data (All distances are in meters.).

Parameters of cylinder	*Gravitational horizontal cylinder*
Distance between depth and axis of the cylinder, z_0	25
Horizontal location relative to the origin, x_0	200
Density contrast (g/cm^3)	2.5
Radius of cylinder	5
Transverse extension	50
Structural index	2
Noise	Random, 2%

In Figure 3(a), the depiction pertains to the Bouguer observation of synthetic gravity data for a horizontal cylinder. This data encompasses 2% random Gaussian noise and is situated at the coordinates (x_0, z_0) = (200, 25) m, accompanied by a density contrast of 2.5 g/ cm^3. In Figure 3(b), it is evident that the DEXP transformation operates with precision, exhibiting minimal variance from the established field values at the corresponding depth.

The attributes of a magnetic cylinder, derived from synthetic data and characterized by uniform and inductive magnetization, are presented in Table (4). The orientation of the measurement axis is perpendicular to the structure.

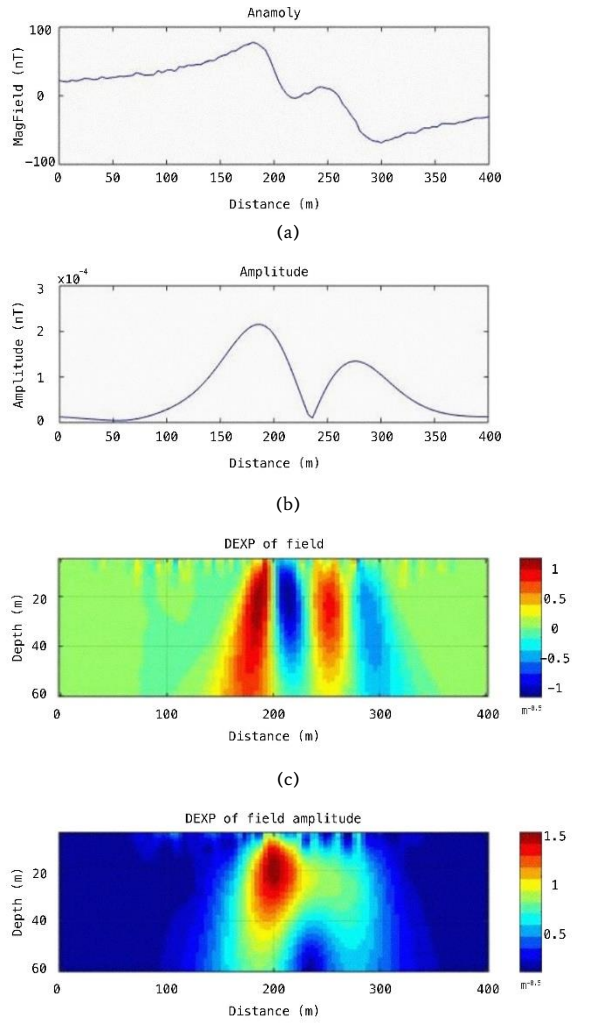

Figure 2 Synthetic magnetic data of two thin dikes, (a) total field observation, (b) amplitude data, and DEXP transformation from the total field (c) and amplitude data (d). Observations were corrupted with 1% random Gaussian noise.

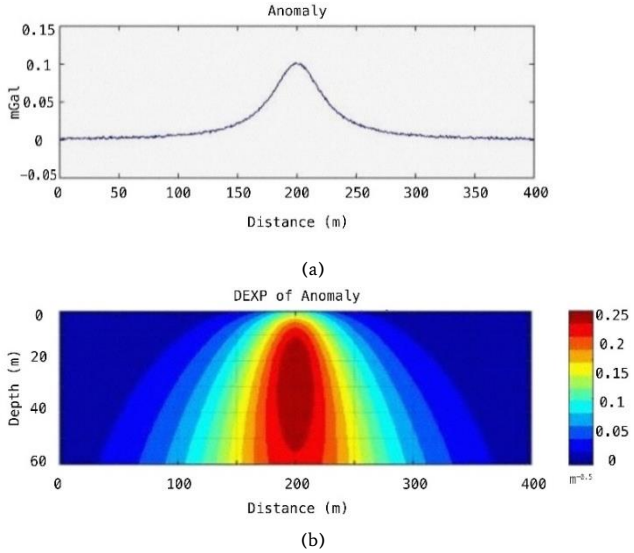

Figure 3 Synthetic gravity data of a cylinder, (a) Bouguer observation, (b) DEXP transformation. Observations were corrupted with 2% random Gaussian noise.

Table 4. Characteristics for a cylinder used to generate magnetic data (all distances and angles are in meters and degrees, respectively).

Parameters of cylinder	*Horizontal magnetic cylinder*
Distance between depth and axis of the cylinder, z_0	20
Horizontal position relative to the origin (meters), x_0	200
Azimuth profile	0
Radius of cylinder	5
Dipole magnetic moment	2
The inclination angle of the earth field, I	45
Earth field declination angle, D	10
Total magnetization inclination, I'	45
Total magnetization declination angle, D'	10
Structural index	2
Noise	Random, 1%

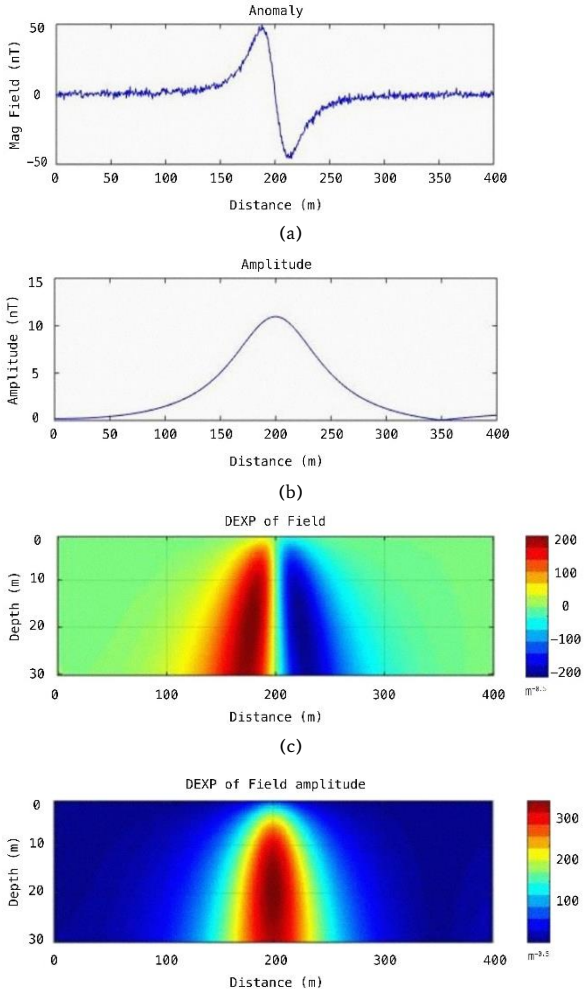

Figure 4 Synthetic magnetic data of a cylinder, (a) total field observation, (b) amplitude data, and DEXP transformation from the total field (c) and amplitude data (d). Observations were corrupted with 1% random Gaussian noise.

After applying the DEXP transformation to the magnetic anomaly originating from the horizontal magnetic cylinder, the outcomes from synthetic magnetic data of the cylinder are illustrated in Figure 4. The figures include (a) the total field observation, (b) amplitude data, and DEXP transformation derived from the total field (c) and amplitude

data (d). Furthermore, the DEXP transformation was employed to assess the magnetic field of a cylinder characterized by a depth of 20 m and a magnetization of 2 A/m. The magnetic field's inclination and declination are set at 45° and 10°, respectively. Figure 4 visually represents an accurate determination of the depth and boundaries achieved through the simulation of a synthetic magnetic cylinder. It is noteworthy that the DEXP transformation provides a reliable estimation of the correct depth, consistently well-approximated across its boundaries. This satisfactory assessment is facilitated by the inherent independence of the local wavenumber DEXP from the structural index value.

5. Geological setting

The Ghareh-Aghaj salt dome is situated in the northwestern vicinity of Mahneshan city, in the northwest region of Zanjan Province, Iran. This study area is positioned on the geological map of Takht-e Suleiman and falls within the central Iran zone. The topography of the region is characterized by open anticlines and expansive synclines, while the slope of the strata varies from nearly horizontal to vertical. As a result, the prevalent landforms comprise rounded hills dotting open plains, featuring sandstone formations and cliffs that overlook valleys.

Within the Ghareh-Aghaj region, the sedimentary deposits consist of siliceous detrital layers, interspersed with thin strata of sandstone and thicker strata of marl. Additionally, conglomerate sediments are intercalated, accompanied by substantial layers of halite exhibiting scattered gypsum layers. Particularly noteworthy, approximately 90% of the sedimentary sequence is composed of thick halite strata [20].

The specific excavation site can be approximately pinpointed at coordinates x=720070 meters and y=4091750 meters. Subsequently, in the following sections, Figures 5 and 6 provide visual representations, showcasing the distribution map of potash resources and a simplified geological map of the Ghareh-Aghaj region in the northwestern part of Iran, respectively.

Potash minerals are typically found within the initial sedimentary layers of evaporite deposits, often occurring in the deeper segments of sedimentary basins. The exploration of potash within known evaporite deposits involves a comprehensive analysis of salt layers through both physical and chemical methodologies.

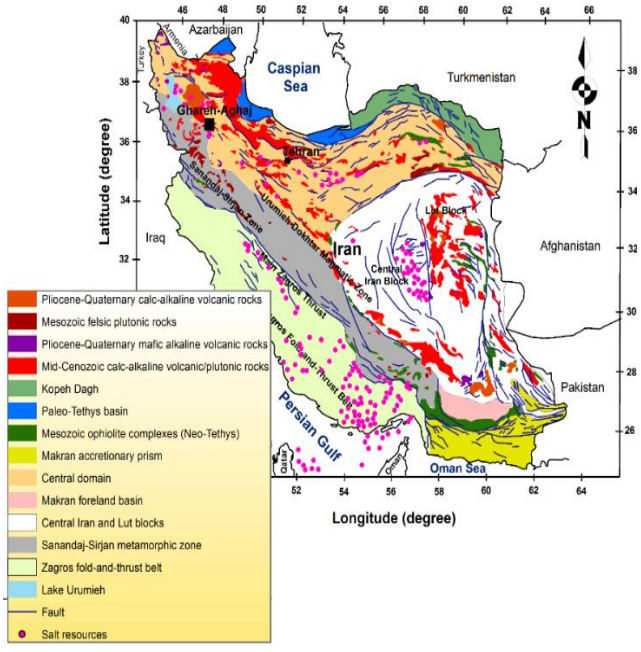

Fig.ure 5. Distribution map of Potash resources in Iran [21].

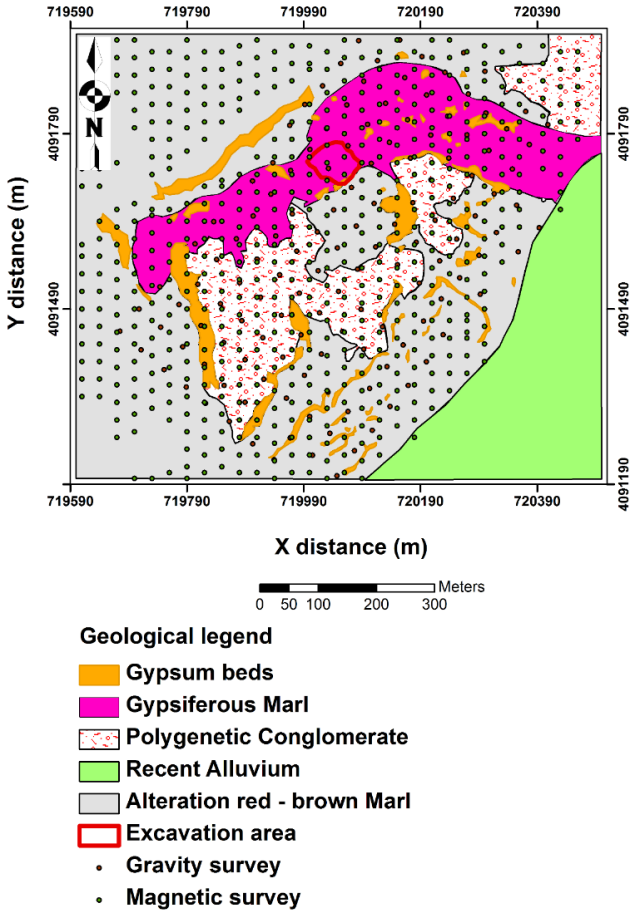

Figure 6. The simplified geological map of the Ghareh-Aghaj at NW of Iran (Reproduced from Geological Survey of Iran, GSI).

Several critical indicators guide potash exploration efforts. These include assessing the thickness of salt sequences, examining the presence of potassium within sedimentary layers, observing variations in salt coloration, and identifying the occurrence of bromine halite.

It's noteworthy that the ionic ratio of sodium to potassium in seawater is approximately 27.7 to 1. This ratio contributes to the coexistence of potassium reserves alongside extensive salt layers. Interestingly, there are instances where salt deposits encircle potash layers due to underlying tectonic processes. Certain geological features such as salt domes, salt springs, and the presence of potassium in specific layers provide valuable clues for detecting potential potash deposits.

Notably, the exploration of potash is closely intertwined with salt exploration, as both minerals share the same geological basin. Detecting the presence or absence of potash requires employing a combination of chemical and physical analysis techniques to detect the underlying geological characteristics.

In summation, the exploration results reveal a distinctive geological feature within the Ghareh-Aghaj salt structure. Positioned along the northern margin, this geological structure manifests as a local anticline characterized by an inclined axial surface facing northward. Notably, the salt intrusion occurred within the Miocene marls, following a predominant north-south trajectory.

6. Geophysical investigations for Potash exploration

Geophysical investigations encompassing magnetometric and gravimetric surveys have been systematically conducted across this region. The primary focus of gravimetric analyses within this area has been to delineate regions exhibiting lower density characteristics. Given

the notably low density of salt domes, the method offers the potential to discern the presence of subsurface salt structures. The initial steps involved gravity corrections employing Nettleton's approach, yielding a regional average density of 2.4 g/cm³.

The outcomes of the gravimetric investigations are manifested in key maps, namely the Bouguer data map and the analytic signal map of the Bouguer data. Referencing Figures 7 and 8, respectively, these maps distinctly illustrate the Ghareh-Aghaj region. Notably, the identified center of the salt dome corresponds approximately to the coordinates x=720180 and y=4091631. The range between the minimal and maximal values within this mapped region is recorded at 2.8 mGal. Thus, a comprehensive inference can be drawn that the insights garnered from the gravimetric approach have efficaciously illuminated the presence of the salt dome.

In addition to the gravimetric approach, the magnetometric method has also been employed to decipher the geological characteristics of the area. Salt domes, being characterized by diamagnetic properties in comparison to surrounding formations, can potentially be differentiated through regions exhibiting diminished magnetism. However, it is noteworthy that the efficacy of the magnetometric method was compromised by the presence of conglomerate formations. The significant fluctuations in magnetic field intensity exceeding 100 gammas contributed to the masking of other regional anomalies.

Despite these challenges, magnetic mapping efforts have yielded valuable insights over the Ghareh-Aghaj region. This is evident in the observed magnetic data, the 20-meter upward continued Reduced-To-Pole (RTP) data, and the analytic signal map of the 10-meter upward continued RTP data, showcased in Figures 9, 10, and 11 respectively. These visual representations collectively shed light on the distribution of conglomerates within the region, which is prominently delineated by a distinct reddish color.

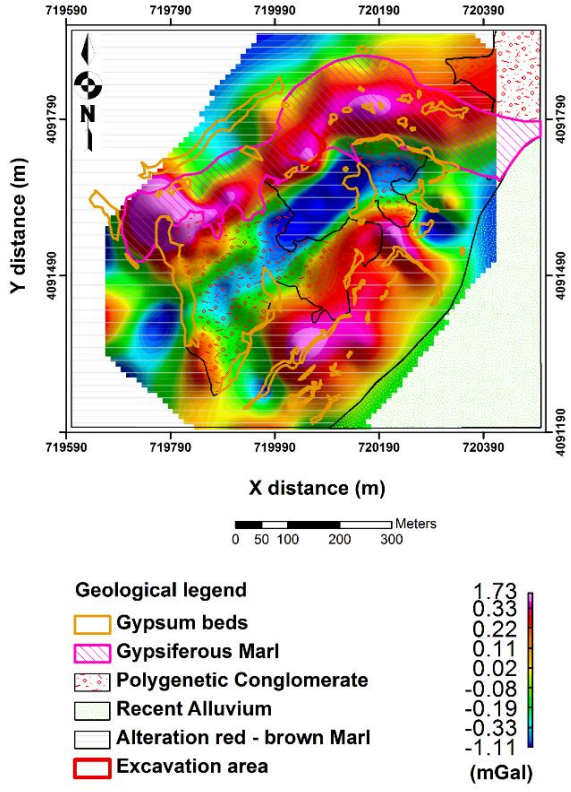

Figure 7. The observed Bouguer data over the Ghareh-Aghaj at NW of Iran. The main geological units have been superimposed on the map.

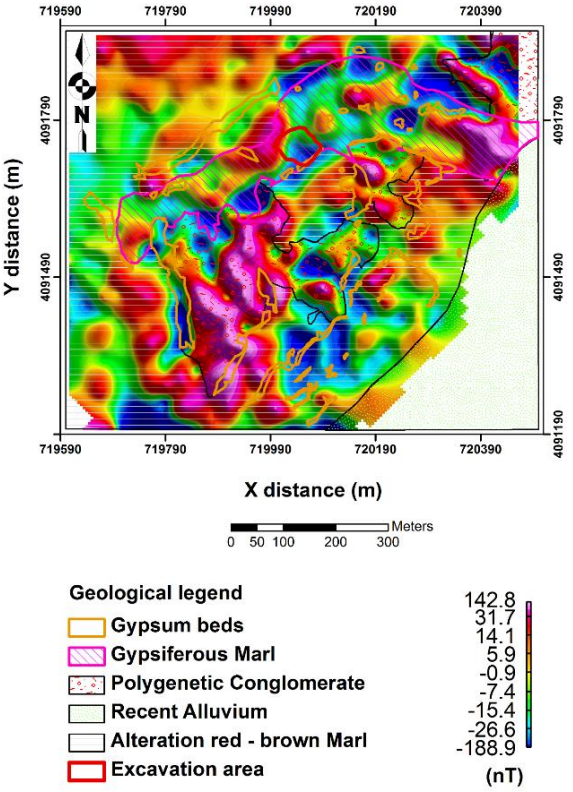

Figure 9. The observed Magnetic data over the Ghareh-Aghaj at NW of Iran. The main geological units have been superimposed on the map.

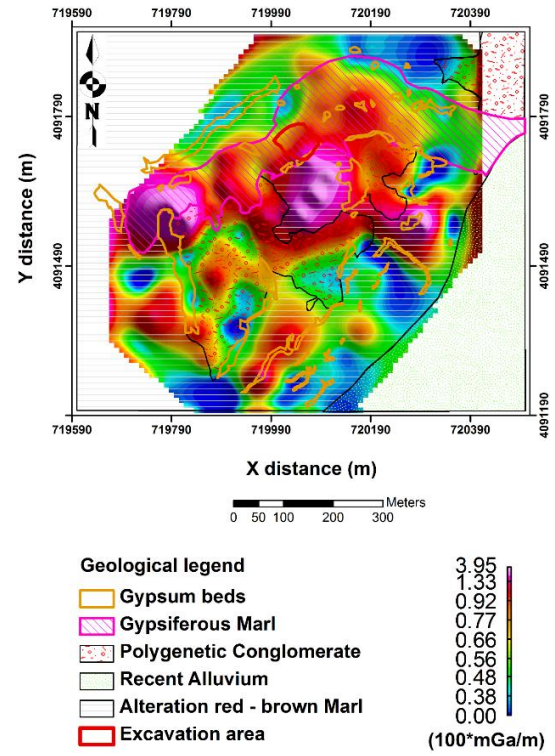

Figure .8. The analytic signal map of the Bouguer gravity data over the Ghareh-Aghaj at NW of Iran and its geological units.

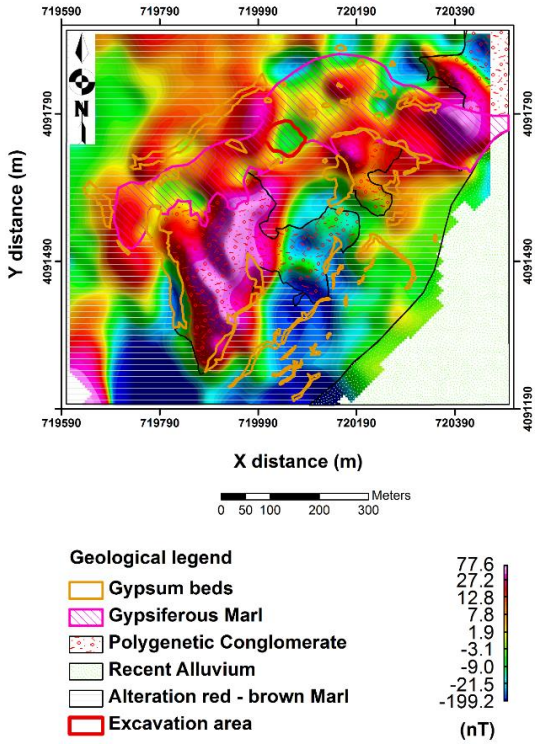

Figure 10. The 20-m upward continued RTP magnetic map over the Ghareh-Aghaj at NW of Iran and its geological units.

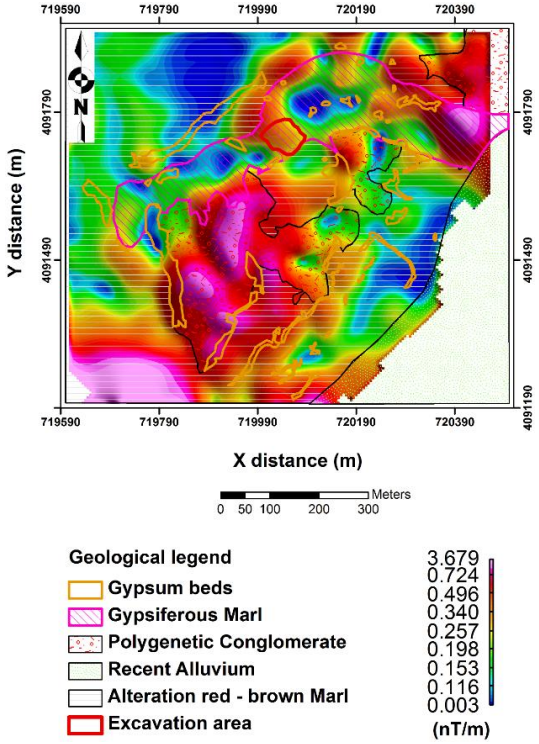

Figure 11. The analytic signal map of the 10-m upward continued RTP data over the Ghareh-Aghaj at NW of Iran and its geological units.

At first, a potential location for additional research and drilling operation was discovered after merging the information related to the region's 1:1000 topographic, magnetic, and gravimetric data with a 1:1000 geological map. It was also determined that the acquired area's approximate extent was somewhere between 220 × 250 square meters when applying the analytical signal method. Then the target range is studied by employing the automatic DEXP transformation. For this purpose, the multiscale analyses are produced by the upward continuation of the potential field and its derivatives. Then, the structure depth is automatically estimated by extracting vertical sections in the direction of the coordinate axes. With this method, there is no limit to the vertical sections and profiles created. Also, the structural index can be estimated with the help of the scaling function along the determined magnetic field boundaries and the amplitude of the total field derivative [13].

It is required to transfer the data to a higher level by operating an upward continuation filter before implementing the DEXP technique to reduce the effects of surface masses and noise; hence, this filter was executed on the data. The optimum height in the upward continuation is the first height, after which the range of changes in depth and the structural index becomes insignificant. Furthermore, the inaccuracy of estimating the source position based on the location of the extreme points of the DEXP transformation can be significantly reduced by employing a reduction to the pole (RTP) filter on the magnetic data. Finally, since the potential fields strongly interfere with each other, it is necessary to use higher-order derivatives to reduce the interference effects, increase the resolution, and to better estimate the depth and the position of the sources [22].

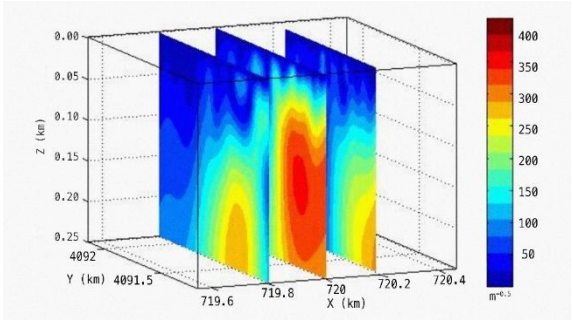

(a)

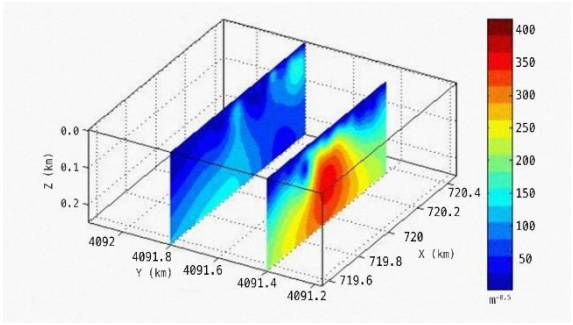

(b)

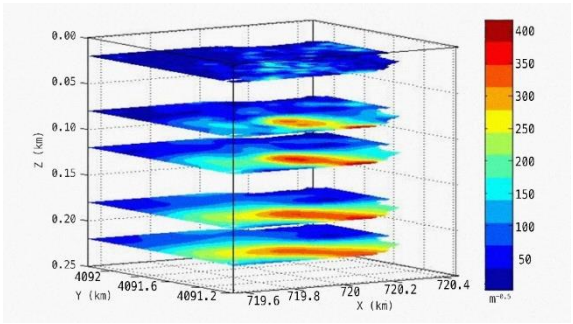

(c)

Figure 12. DEXP imaging of magnetic data along the x-axis (a), y-axis (b) and z-axis (c). Amplitude data were utilized.

Illustrated in Figure 12, is the DEXP imaging outcome derived from magnetic data. The magnetic field's inclination and declination angles are set at 50 and 5 degrees, respectively. To refine the magnetic field data, an IGRF correction using the value of 47,700 was implemented. The process of upward continuation was carried out at heights ranging from 1 to 250 meters. Furthermore, the structural index of 2, aligned with the salt dome's structure, was employed.

Similarly, the DEXP methodology was extended to gravity data, as depicted in Figure 13. This comprehensive approach allows for the visualization and analysis of both magnetic and gravity data, contributing to a more holistic understanding of the geological characteristics of the study area.

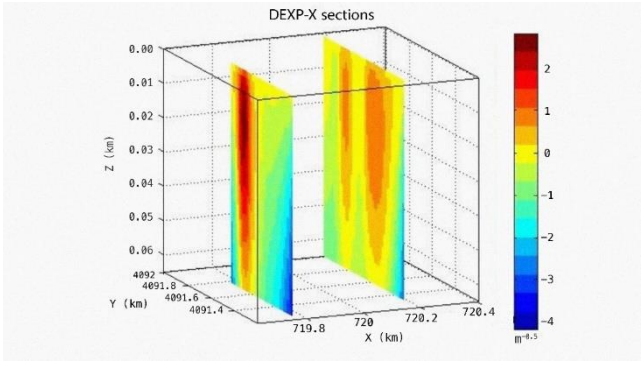

(a)

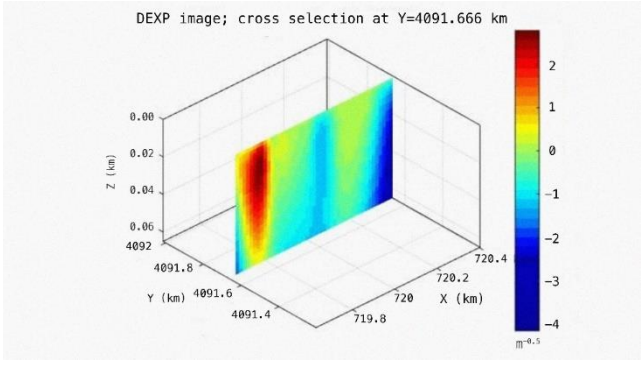

(b)

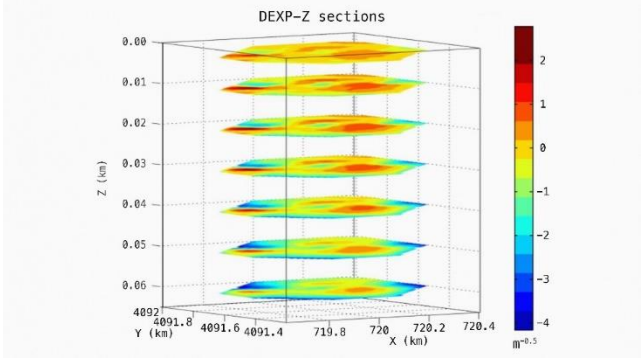

(c)

Figure 13. DEXP imaging of gravity data along the x-axis (a), y-axis (b), and z-axis (c).

By integrating the potential maps and the DEXP imaging results obtained for the Ghareh-Aghaj region (depicted in Figures 12 and 13), the salt dome anomaly is clearly discernible in the northeastern to southwestern orientation. This anomaly extends over approximately 200 meters in length and is situated at depths ranging from around 20 to 100 meters. The sedimentary layers comprising the anomaly's structure have an overall thickness of approximately 40 meters.

As previously mentioned, the vulnerability of responses to noise augmentation, typically observed in derivative-based methodologies, is mitigated in the DEXP transformation due to the implementation of a low-pass filter through upward continuation. Consequently, variations in noise levels do not significantly impact the DEXP transformation's outputs, thereby enhancing its credibility and acceptance in comparison to other techniques. The inherent stability of the DEXP transformation, particularly in relation to noise levels and the order of field derivatives, stands out as a prominent attribute. This stability is grounded in the inherent behavior of potential fields with respect to elevation changes. As a result, the DEXP transformation exhibits applicability even to hypothetical derivative fields with elevated orders, enhancing resolution and the accuracy of parameter estimation for various source types. Consequently, the reliability of the outcomes rests heavily on the precision of the initial measurement data, underscoring the importance of high-quality data acquisition.

In the final phase, in line with the exploration objectives, including determining the direction of the anticline axis within the salt dome area, identifying potential potash concentrations along the folds' axis, and locating potash springs, five initial drilling sites were designated. These points were strategically placed around the salt dome, forming a radial arrangement.

To execute the drilling plan, a network of five boreholes was established. Among them, three boreholes were inclined, while two were drilled vertically. The borehole depths ranged from 100 to 120 meters, totaling 551.05 meters of drilling. Importantly, the drilling directions varied between 0 and 345 degrees, with horizontal drilling slopes ranging from 0 to 10 degrees [20].

Briefly, as shown in Fig. 14, the depth profiles of four crucial boreholes provide valuable insights:

BH1, drilled at coordinates x=720307 and y=4091847, reaches 102.1 meters depth with a slope of 80 degrees and azimuth of 270 degrees. The lithology encompasses marl up to 58.5 meters, followed by salt layers, transitioning to an alternation of marl and sandstone until 102 meters.

BH2, located at x=720016 and y=4091765, extends 120 meters deep. With a slope of 180 degrees and azimuth of 145 degrees, lithology commences with marl up to 12.5 meters, thereafter featuring continuous salt layers.

BH4, vertically drilled at x=720040 and y=4091854, achieves a depth of 116.2 meters. The lithological sequence comprises alternating sections of sandstone, silt, and gypsum up to 11.7 meters, transitioning into continuous salt layers.

BH5, positioned at x=719913 and y=4091740, has a depth of 100.5 meters, with a slope of 85 degrees and azimuth of 345 degrees. The lithology commences with marl up to 11.4 meters, followed by consistent salt layers [20].

7. Conclusion

The core objective of this study was to explore the effectiveness of the automatic DEXP transformation method in analyzing potential field data for depth determination. Through its application on synthetic models, the DEXP technique demonstrated its capability to reasonably estimate relevant properties. This suggests that the DEXP transformation can serve as an initial step in identifying potential field anomalies and conducting geophysical analyses, serving as a fundamental building block before employing more intricate modeling techniques. Moreover, it's common practice to employ multiple approaches to enhance the accuracy and reliability of potential field data evaluation and interpretation. This integrated approach contributes to minimizing errors and strengthening the overall credibility of the findings. Furthermore, in alignment with the geophysical surveys of potential fields carried out in the area and the DEXP imaging of the salt-bearing anticline, findings align with the drilling results. It's evident that the salt's lateral spread is limited, focusing on greater depths. The salt structure demonstrates an elongation of approximately 200 meters along its length, reaching depths of 20 to 100 meters, with a thickness of around 40 meters.

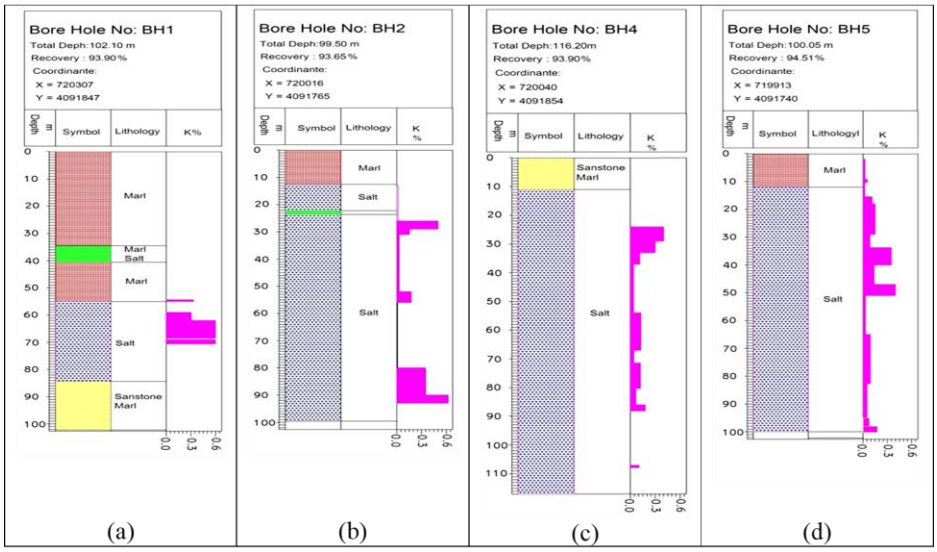

Figure 14. Depth section of four drillings, (a) BH1, (b) BH2, (c) BH4, and (d) BH5. Reproduced from GSI.

Acknowledgments

The authors express their gratitude to the Geological Survey of Iran (GSI) for generously providing the necessary data for this study.

REFERENCES

[1] Nabighian M.N, Grauch V.J.S, Hansen R.O, Lafehr T.R, Li Y, Peirce J.W, Phillips J.D, Ruder M.E (2005) Historical development of the magnetic method in exploration. Geophysics 70: 33ND-61ND.

[2] Nabighian M.N (1972) The analytic signal of two-dimensional magnetic bodies with polygonal cross-section: its properties and use for automated anomaly interpretation. Geophysics 37: 507-517.

[3] Thurston J.B, Smith R.S (1997) Automatic conversion of magnetic data to depth, dip, susceptibility contrast using the SPI method. Geophysics 62: 807-813.

[4] Fedi M, Rapolla A, Russo G (1999) Upward continuation of scattered potential field data. Geophysics 64: 443-451.

[5] Thompson D.T (1982) EULDPH: A new technique for making computer assisted depth estimates from magnetic data. Geophysics 47: 31-37.

[6] Reid A.B, Allsop M, Granser H, Millet A.J, Somerton W (1990) Magnetic interpretation in three dimensions using Euler deconvolution. Geophysics 55: 80-91.

[7] Stavrev P, Reid A.B (2007) Degrees of homogeneity of potential fields and structural indices of Euler deconvolution. Geophysics 72: L1-L12.

[8] Salem A, Ravat D (2003) A combined analytic signal and Euler method AN-EUL for automatic interpretation of magnetic data. Geophysics 68: 1952-1961.

[9] Salem A, Ravat D, Smith R, Ushijima K (2005) Interpretation of magnetic data using an enhanced local wavenumber (ELW) method. Geophysics 70: 141-151.

[10] Smith R.S, Thurston J.B, Dai T.F, MacLeod I.N (1998) ISPITM—the improved source parameter imaging method. Geophys. Prospect. 46 (2): 141–151.

[11] Fedi M (2007) DEXP: a fast method to determine the depth and the structural index of Potential field sources. Geophysics 77(1): G13-G24.

[12] Fedi M, Florio G, Quarta T (2009) Multiridge analysis of potential fields: Geometric method and reduced Euler deconvolution. Geophysics 74(4): L53-L65.

[13] Fedi M, Pilkington M (2012) Understanding imaging methods for potential field data. Geophysics 77(1): G13-G24.

[14] Abbas M.A, Fedi M, Florio G (2014) Improving the local wavenumber method by automatic DEXP transformation. Journal of Applied Geophysics 111: 250-255.

[15] Bracewell R (1965) The Fourier transform and its applications. McGraw-Hill Book Co.

[16] Phillips J.D, Hansen R.O, Blakely R.J (2007) The use of curvature in potential-field interpretation. Exploration Geophysics 38(2): 111–119.

[17] Telford W.M, Geldart L.P, Sheriff, R.E (1990) Applied Geophysics. Cambridge University Press.

[18] Mushayandebvu M.F, van Driel P, Reid A.B, Fairhead J.D (2001) Magnetic source parameters of two-dimensional structures using extended Euler deconvolution. Geophysics, 66, 814-823.

[19] Blakely RJ (1995) Potential Theory in Gravity and Magnetic Applications. Cambridge Univ. Press.

[20] Razavi S.A, Jafari F (2008) Report of potash explorations employing magnetometric and gravimetric techniques in Aji-Chai and Ghareh-Aghaj areas. Geological Survey and Mineral Exploration of Iran.

[21] Abedi M (2018) An integrated approach to evaluate the Aji-Chai potash resources in Iran using potential field data. Journal of Applied Geophysics, 139, 379-391.

[22] Abedi M., Oskooi B (2015) A combined magnetometry and gravity study across Zagros orogeny in Iran. Tectonophysics, 664, 164-175.